Automatic Detection of Bridge Deck Condition From Ground Penetrating Radar Images

Zhe Wendy Wang, *Member, IEEE*, Mengchu Zhou, *Fellow, IEEE*, Gregory G. Slabaugh, *Senior Member, IEEE*, Jiefu Zhai, *Member, IEEE*, and Tong Fang

***Abstract*—Accurate assessment of the quality of concrete bridge decks and identification of corrosion induced delamination lead to economic management of bridge decks. It has been demonstrated that ground penetrating radar (GPR) can be successfully used for such purposes. The growing demand on GPR has brought into the challenge of developing automatic processes necessary to produce a final accurate interpretation. However, there have been few publications targeting at automatic detection of bridge deck delamination from GPR data. This paper proposes a novel method using partial differential equations to detect rebar (or steel-bar) mat signatures of concrete bridges from GPR data so that the delamination within the bridge deck can be effectively located. The proposed algorithm was tested on both synthetic and real GPR images and the experimental results have demonstrated its accuracy and reliability, even for diminished image contrast and low signal-to-noise ratio. Therefore, an accurate deterioration map of the bridge deck can be generated automatically.**

***Note to Practitioners*—This work was motivated by the problem of automatic detection of delamination inside a bridge deck. Nowadays, to generate the final bridge condition report from GPR data still relies on experienced civil engineers' excessive intervention and scan-by-scan processing. Therefore, the current method is both time and labor-consuming. Moreover, it has limited reproducibility and is subject to an operator's variability. This work presents a new approach to automatically generate the bridge deterioration report. It derives mathematical equations to fit the rebar shape in GPR images and applies the results to real data. The rebar inside the bridge deck can be detected accurately in spite of the low signal-to-noise ratio and low contrast. The final deterioration map is then generated based on the corroded rebar detection results automatically. This work is already tested and used in a real bridge in New Jersey, U.S.A.**

***Index Terms*—Automatic detection, ground penetrating radar (GPR), image processing, partial differential equations (PDEs).**

I. Introduction

THE I-35 highway bridge collapsed into the Mississippi River, in Minneapolis, MN, during the evening rush hour on August 1, 2007. Approximately 100 vehicles were involved and 13 deaths were attributed to the collapse. This tragedy signifies that the condition of the bridges in the United States is deteriorating and requires enormous financial and human resources for its maintenance and mitigation. An important component of the inspection and rehabilitation of concrete bridges is the assessment of the bridge deck condition. The advent of nondestructive evaluation techniques has significantly aided this task, and several methods have been successfully utilized to detect common defects in concrete bridge decks. Among these methods, Ground Penetrating Radar (GPR) is one of the most widely used techniques nowadays.

Accurate assessment of the quality of concrete bridge decks and identification of corrosion induced delamination are very important research topics. They can lead to economic management of bridge decks. Romero *et al.* have demonstrated that GPR can be successfully used for such purposes [2]. There is a growing need to develop automatic processes necessary to produce a final accurate interpretation from GPR data.

While it is capable of detecting deck delaminations at various stages of deterioration, precise interpretation of the measured parameters has yet to be fully automated. The postprocessing procedures leading to the final interpretation still suffer from some drawbacks, such as excessive reliance on experienced operators' intervention and scan-by-scan processing. Significant improvements to the automation of a bridge condition evaluation process are expected to come from imaging and image processing techniques.

On the GPR section, potential areas of deterioration appear as zones of signal attenuation. Delamination is most likely to occur around rebar mats within the concrete. Typically, corroded rebar area has a lower dielectric constant than normal rebar area, producing an incoherent/weaker reflection on the GPR section. Therefore, the amplitude of reflection and attenuation are measured as an indication of delamination of the rebar mat from the concrete and deterioration of the concrete. Our work is targeting at the automatic detection of bridge deck delamination.

A crucial component of automatic bridge condition evaluation is the detection of corroded rebars, as delamination always

Manuscript received February 04, 2010; revised August 28, 2010; accepted September 19, 2010. Date of publication December 20, 2010; date of current version July 07, 2011. This paper was recommended for publication by Associate Editor P. Sastry and Editor Y. Narahari upon evaluation of the reviewers' comments. This paper was supported in part by the National Basic Research Program of China under contracts 2008AA04Z109, and 2011CB302804, and Chang Jiang Scholars Program, PRC Ministry of Education. This paper was presented in part at the 2008 IEEE International Conference on Automation Science and Engineering, Washington, DC, August 2008.

Z. W. Wang is with Iris ID Systems, Inc. (formerly LG Iris), Cranbury, NJ 08512 USA (e-mail: joywangzhe@hotmail.com; zhe.joywangzhe@gmail.com).

M. Zhou is with The MoE Key Laboratory of Embedded System and Service Computing, Tongji University, Shanghai 200092, China (e-mail: mengchu@ieee.org).

G. G. Slabaugh is with Medicsight PLC, Kensington Centre, London, W14 8UD, U.K. (e-mail: greg.slabaugh@medicsight.com).

T. Fang is with the Real-Time Vision and Modeling Department, Siemens Corporate Research, Princeton, NJ 08540 USA (e-mail: tong.fang@siemens.com).

J. Zhai is with Apple Inc., Cupertino, CA 95014-2084 USA (e-mail: jeffzhai@gmail.com).

Color versions of one or more of the figures in this paper are available online at http://ieeexplore.ieee.org.

Digital Object Identifier 10.1109/TASE.2010.2092428

occurs around rebars. Due to the GPR imaging principle, the reflected wave feature of the rebar mat is a series of hyperbolas and the top of each hyperbola denotes the corresponding rebar's position. Despite its importance, however, there is a limited amount of literature that can be found about hyperbolas series specific fitting algorithm for GPR data from a bridge deck.

Cylindrical objects such as buried pipes appear in the GPR images as hyperbolas. There have been several hyperbolic signature detection methods in literature for the applications such as detection of distinct landmine or buried pipe. Among them, migration is a commonly used frequency-domain method and it collapses hyperbolas into short linear regions [3]. Another trend is using neural network or fuzzy logic to detect arc signatures in GPR scans [4]–[8]. However, few of these methods are devised for the corroded rebar mats in concrete bridges, which is much more difficult to detect than the ordinary buried utilities. Most GPR-related data processing work tends to rely on less sophisticated techniques for hyperbolic signature detection, and thus suffers from drawbacks caused by noise, such as the detector in [9], being only able to detect good and good-minus signatures, which is not suitable for delamination detection.

In this paper, we propose a novel method based on partial differential equations (PDEs) to discriminate rebar mat signatures for bridge deck delamination detection in GPR images. We first detect the apex of each rebar using a template-based method with a similarity metric of sum of squared difference (SSD) and then estimate the parameters of each hyperbola in the GPR images with a PDE method. Based on the rebar detection result, deterioration map of bridge decks can be generated automatically for maintenance and rehabilitation guidance. We also perform a comparison study of the proposed method with the traditional manual approach in condition assessment of bridge decks.

The rest of this paper is organized as follows. Section II gives a brief review of GPR history and describes the characteristic shape of rebar signatures in GPR images. Section III proposes a novel PDE-based rebar detection method. Section IV provides results that demonstrate the ability of the proposed method to detect rebar signatures in GPR images, even for images of diminished contrast and low signal-to-noise ratio (SNR). Section V provides the deterioration map of the test bridge with our automatic method. Section VI concludes this paper.

II. Ground Penetrating Radar (GPR)

A. History and Applications of GPR

The history of GPR applications in transportation infrastructure surveys dates back to the early and mid 1970s when the Federal Highway Administration (FHWA) in the U.S. tested its feasibility in tunnels, bridge decks applications [10] and for moisture detection in construction materials [11]. Later on, GPR use was expanded to encompass bridge deck inspection [12] and void detection under concrete highways. In the late 1980s and early 1990s, most infrastructure applications in North America focused on pavement thickness measurements, detecting voids under concrete slabs and detecting deteriorated areas in bridge decks [13], [14].

The real exploration in the advancement of GPR occurred in the mid and late 1990s. Many groups worldwide began to show great interests in this technology. On the commercial side, during this time, Geophysical Survey System Inc. (GSSI) (USA) gained considerable commercial success. Besides GSSI, other leading commercial manufacturers of GPR showed up as well, such as Mala (Sweden), Roadscanners (Finland), IDS (Italy), Penetradar (U.S.), Sensors and Software (Canada), and UTSI Electronics (U.K.).

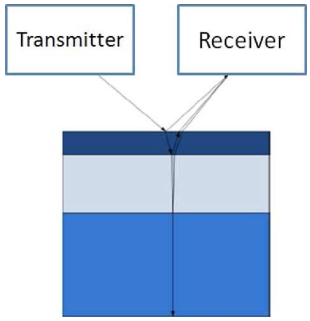

Fig. 1. Basic principle of a GPR technique.

On the academic side, more attention started to be paid by both geophysical and electrical engineering communities two decades ago. Techniques like digital data processing and 2D numerical simulation have been developed since then [15]. 3D numerical modeling is performed [16]. Besides, civil engineering professionals have focused on gaining a more detailed understanding of the relationship between the dielectric properties and permanent deformation properties of unbound materials [17]. In the image processing/computer vision field, researchers have been putting much effort on object detection, such as mines and utilities from GPR images.

The history of GPR is intertwined with diverse applications of the technique. Currently, the most common applications of GPR in bridge surveys include: 1) Bridge deck condition assessment; 2) Determining concrete cover depth on new structures; 3) Measuring bridge deck thickness; 4). Locating metallic and nonmetallic targets in concrete; 5) Void detection and location; and 6) Inspection of other reinforced concrete structures.

During the past decade, the development on GPR was focused on various applications in bridge inspection. Among them, GPR seemed to be the most successful for pavement layer thickness measurements, while agencies reported less satisfactory results with void detection and questionable results locating the areas of delamination [10]. Recently, the focus has been on collecting reflection amplitude data from bridge decks and preparing "deterioration maps" that present damaged areas in the bridge structures [18].

B. Basic Principle of GPR

A GPR system uses a radio wave source with a central frequency varying from 10 MHz up to 2.5 GHz to transmit a pulse of electromagnetic energy into the medium. When the pulse reaches an electric interface in the medium, some of the energy is reflected back while the rest proceeds forwards. The reflected energy, originating within the medium at interfaces between materials of different dielectric properties or of differing conductivities, is received and recorded for the analysis of internal structure of the medium, as illustrated in Fig. 1. The reflected energy is collected and displayed as a waveform showing

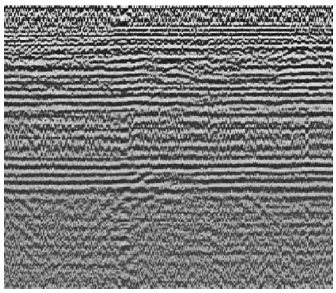

Fig. 2. An example of GPR image (color print is preferred).

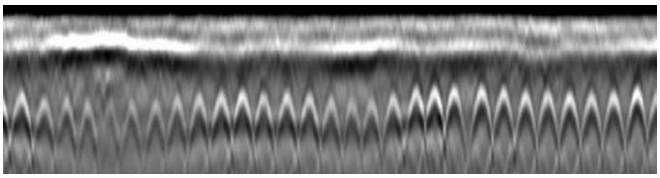

Fig. 3. Rebar signature in a GPR image.

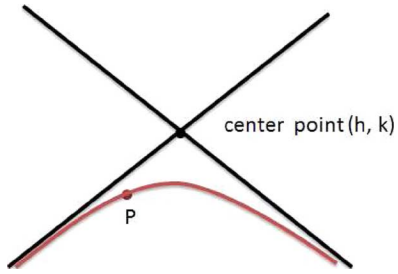

Fig. 4. Hyperbola profile.

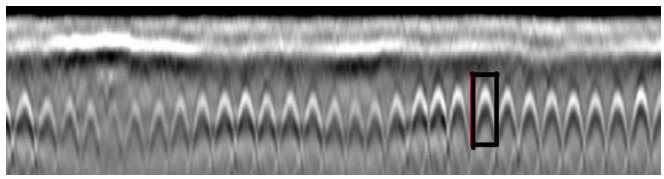

Fig. 5. A rebar template in a GPR image.

amplitudes and time elapsed between wave transmission and reflection. When the measurements are repeated and the antenna is moving, a continuous profile is obtained across the target, as depicted in Fig. 2.

GPR data usually consist of: 1) changes in reflection strength; 2) changes in arrival time of specific reflections; 3) source wave distortion; and 4) signal attenuation.

When applied to the analysis of bridge decks, these different GPR signatures can be used for detecting internal corrosion of steel reinforcement within the concrete deck. They can be considered as an indicator of poor quality overlay bonding or delamination at the rebar level.

Although no imaging of debonding or delamination is measured directly with GPR, the radar reflection character is related directly to the amount of debonding/delamination, which allows (chloride-bearing) fluids to reach the rebar mat.

C. Hyperbolic Signatures

Locating rebar mat is usually done by noting hyperbolic shapes in the GPR image, as indicated in Fig. 3 (color printout is needed for better readability for all figures). A series of hyperbolas are shown in the GPR image, with some of the hyperbolic signatures being blurred. The apex of each hyperbola locates each rebar. These hyperbolas occur due to the reason that the antenna transmits energy in a spatially varying pattern that can be approximated to a cone. Consequently, it receives reflections from the rebar at decreasing two-way travel time as it approaches the rebar, then increasing the travel time after passing over the rebar. Areas of the rebar mat exhibiting weak reflection amplitude are typically indicative of deterioration.

A hyperbolic rebar signature can be described by a simple geometrical function. For example, let a point $\mathbf{p}$ in a south-opening hyperbola (concave) be expressed as

$$\mathbf{p} = \begin{bmatrix} x \\ y \end{bmatrix} = \begin{bmatrix} x \\ a\sqrt{1 + \frac{(x-h)^2}{b^2}} + k \end{bmatrix} \tag{1}$$

where (x, y) is the coordinate, (h, k) is the center point, a and b are the shape parameters. The asymptotes cross at the center of the hyperbola and have slope $\pm a/b$ for the south-opening hyperbola. The hyperbola profile is depicted in Fig. 4.

It is worth noting that there are four degrees of freedom for the hyperbola profile fitting according to (1), while some researchers use an equation modeling the hyperbolic signatures from GPR data in the form as follows [9], [19]:

$$\frac{y^2}{a^2} - \frac{(x-h)^2}{b^2} = 1. \tag{2}$$

Unfortunately, (2) uses only three degrees of freedom for the hyperbola fitting, which does not suffice to deal with the problem at hand. Moreover, it is based on the assumption that the modeled signatures result from point reflectors, which cannot be guaranteed in the case of a rebar mat.

III. Signature Discrimination Based on PDE

The proposed scheme consists of two major stages: first, using a template based method, we detect the apex of the hyperbolic signatures. Next, we fit the hyperbola curves to the GPR image data using partial differential equations in an iterative fashion, with the initial guess of the center point modified from the apex obtained in the previous step.

A. SSD-Based Hyperbola Center Point Detection

In this step, we use a template, as shown in the box in Fig. 5, to match the rebar signature based on the similarity metric of sum of squared difference (SSD), defined as follows:

$$\text{SSD} = \sum_x \sum_y (T(x,y) - I_w(x,y))^2 \tag{3}$$

where $T(x, y)$ and $I_w(x, y)$ denote the template image and the region over a sliding window in the GPR image, respectively. When these two images are geometrically aligned, the SSD value reaches its minimum. SSD is chosen as it offers sufficient accuracy and is simple to implement.

We first search the minimum SSD values along each column in the whole GPR image and the one that contributes to minimum SSD values is selected as a reference rebar apex position. Since the interval between two adjacent rebars is usually fixed,

we then exploit the periodicity of the hyperbolic signatures so as to detect all the rebars. To determine the periodicity, a commonly used method Fast Fourier Transform (FFT) is applied. Other methods than using FFT can also be used to determine the periodicity. FFT is selected due to its simplicity for implementation. Therefore, with the assistance of reference rebar and periodicity of hyperbolic signatures, apex positions of all the rebars are obtained. Afterwards, the knowledge is incorporated to the PDEs as the initial guess of center point of each hyperbola for the next step.

B. Hyperbolic Signature Discrimination

Our goal is to fit the hyperbola curve l to the GPR image data. To accomplish this, an energy function is designed as

$$E = \int_l I(\mathbf{p}) dl \tag{4}$$

where $I(\mathbf{p})$ is the intensity of pixel $\mathbf{p}$ and the integral is along the hyperbola from point p_1 to p_2. By maximizing this energy function, the intensity of the image data along the hyperbola achieves its maximum. Therefore, the hyperbola curve is fit to the GPR image.

Starting with an initial guess, we can iteratively update the hyperbola parameters using PDEs to maximize the energy function in (4). Note that, we use the position of the hyperbola center point obtained from the previous step as the initial guess of h and k.

Using a chain rule, differentiation of energy function E with respect to parameter a gives

$$\frac{\partial E}{\partial a} = \int_l \nabla I \cdot \frac{\partial \mathbf{p}}{\partial a} dl \tag{5}$$

where ∇I is the gradient of the image, $\partial \mathbf{p}/\partial a = \begin{bmatrix} 0 \\ \partial y/\partial a \end{bmatrix}$.

We solve $\partial y/\partial a$ according to (1) as

$$\frac{\partial y}{\partial a} = \sqrt{1 + \frac{(x-h)^2}{b^2}}. \tag{6}$$

Therefore, $\partial \mathbf{p}/\partial a$ and $\partial \mathbf{E}/\partial a$ are derived as

$$\frac{\partial \mathbf{p}}{\partial a} = \begin{bmatrix} 0 \\ \sqrt{1 + \frac{(x-h)^2}{b^2}} \end{bmatrix} \tag{7}$$

$$\frac{\partial E}{\partial a} = \int_l \nabla I \cdot \begin{bmatrix} 0 \\ \sqrt{1 + \frac{(x-h)^2}{b^2}} \end{bmatrix} dl. \tag{8}$$

In a similar fashion, we can calculate the expressions for $\partial \mathbf{p}/\partial b$, $\partial \mathbf{p}/\partial h$ and $\partial \mathbf{p}/\partial k$. Clearly, $\partial x/\partial b = \partial x/\partial h = \partial x/\partial k = 0$. Next, we derive $\partial y/\partial b$, $\partial y/\partial h$ and $\partial y/\partial k$.

Differentiation of y with respect to b, h and k, can be expressed, respectively, as

$$\begin{aligned} \frac{\partial y}{\partial b} &= a \cdot \frac{1}{2} \cdot \frac{1}{\sqrt{1 + \frac{(x-h)^2}{b^2}}} \cdot (-2) \cdot (x-h)^2 \cdot \frac{1}{b^3} \\ &= -\frac{a(x-h)^2}{b^3 \sqrt{1 + \frac{(x-h)^2}{b^2}}} \end{aligned} \tag{9}$$

$$\begin{aligned} \frac{\partial y}{\partial h} &= a \cdot \frac{1}{2} \cdot \frac{1}{\sqrt{1 + \frac{(x-h)^2}{b^2}}} \cdot \left(\frac{-1}{b^2}\right) \cdot 2(x-h) \\ &= -\frac{a(x-h)}{b^2 \sqrt{1 + \frac{(x-h)^2}{b^2}}} \end{aligned} \tag{10}$$

$$\frac{\partial y}{\partial k} = 1. \tag{11}$$

Consequently, differentiations of energy function E with respect to parameter b, h, and k give

$$\frac{\partial E}{\partial b} = \int_l \nabla I \cdot \begin{bmatrix} 0 \\ -\frac{a(x-h)^2}{b^3 \sqrt{1 + \frac{(x-h)^2}{b^2}}} \end{bmatrix} dl \tag{12}$$

$$\frac{\partial E}{\partial h} = \int_l \nabla I \cdot \begin{bmatrix} 0 \\ -\frac{a(x-h)}{b^2 \sqrt{1 + \frac{(x-h)^2}{b^2}}} \end{bmatrix} dl \tag{13}$$

$$\frac{\partial E}{\partial k} = \int_l \nabla I \cdot \begin{bmatrix} 0 \\ 1 \end{bmatrix} dl. \tag{14}$$

In order to maximize the energy function, we use a gradient ascent method, i.e.,

$$\mathbf{r}_{n+1} = \mathbf{r}_n - \gamma \cdot \nabla E(\mathbf{r}_n) \tag{15}$$

where $\mathbf{r}_n = \begin{bmatrix} a_n \\ b_n \\ h_n \\ k_n \end{bmatrix}$ and γ is the step-size parameter. Equation (15) is iterated until the maximum number of iteration steps is reached or the prescribed accuracy is met, i.e.,

$$\| \mathbf{r}_{n+1} - \mathbf{r}_n \| \leq \varepsilon \tag{16}$$

where ε is a given small positive value, typically 10^{-6}.

Consider the first step of the algorithm, we assume that the image size (number of pixels) is M and the template size is N. Then, the time complexity is $O(MN)$. Regarding the second step of the algorithm, we assume that the number of rebars is R, obtained from the first step, and the iteration number is I. Then, the time complexity is $O(RI)$.

IV. Experimental Results

In the experiments, we begin with synthetically generated data, designed to study the detection performance as the contrast level is diminished, as depicted in Fig. 6. Here, the contrast refers to the difference in visual properties that makes an object (or its representation in an image) distinguishable from other objects and the background. To quantify the detection performance with respect to the diminishing contrast, which occurs around corroded rebars, we calculate the distance between the ground truth and the detected hyperbolas as the detection error, defined as follows:

$$D = \frac{1}{n} \sqrt{\sum_i^n d_i^2} \tag{17}$$

where n is the number of pixels along the rebar curves and d_i is the Euclidean distance between the ith point in the original

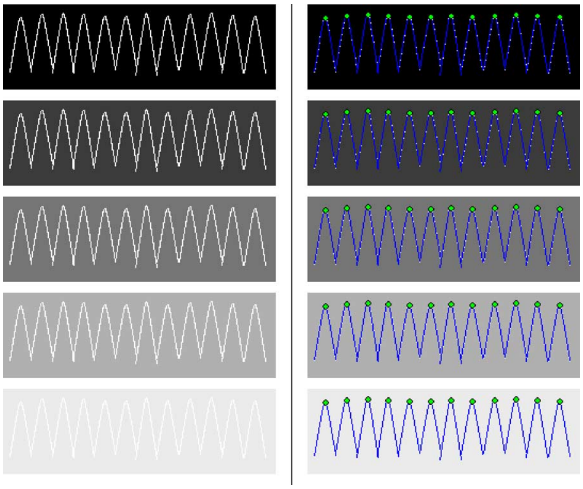

Fig. 6. Rebar detection in synthetic GPR images. The left column shows the original synthetic GPR Images with contrast level being diminished. The right column is the detection results.

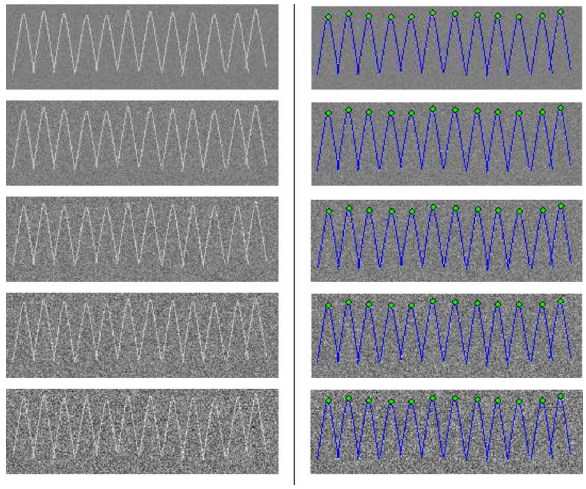

Fig. 8. Rebar detection in synthetic GPR images. The left column is the original synthetic GPR Images with SNR being decreased. The right column is the detection results.

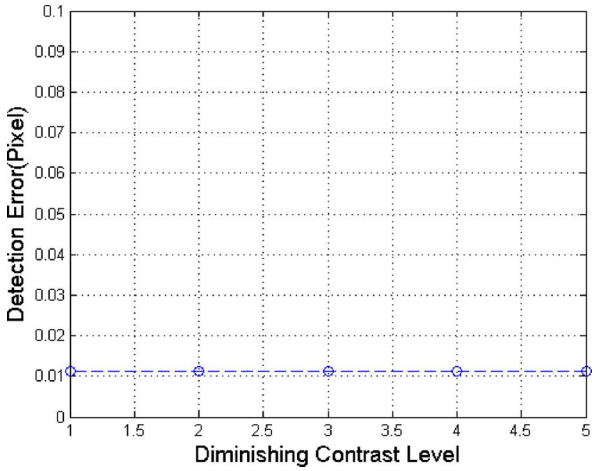

Fig. 7. Detection error as a function of diminishing contrast.

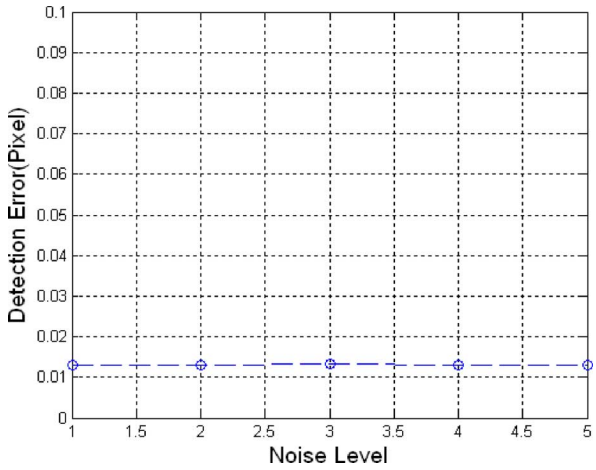

Fig. 9. Detection error as a function of decreased SNR.

hyperbola and the corresponding point in the detected curve. Note that the "ground truth" here means the parameter values of the original hyperbola. From Fig. 7, we can observe that the detection performance does not degrade when the contrast is diminished.

To evaluate the algorithm performance with respect to SNR, we devise another set of experiments, as depicted in Fig. 8. Similarly, we calculate the distance between the ground truth and the detected hyperbolas as the detection error, according to (17). We define the noise level in the image as the standard deviation of the background noise. From Fig. 9, it is obvious to notice that the proposed method is very robust to decreasing SNR or increasing noise level. The detection error is only around 0.013 pixel.

We also examine the effectiveness of the proposed method for real GPR images of bridges, as depicted in Figs. 10(a) and 11(a). The pulse transmitted by GPR is usually displayed in an image as a characteristic dark-light-dark series of bands. The results are fairly clear.

In the original GPR images Fig. 10(a) and (c), there is a section with the amplitude of the signal reflection around the rebar being attenuated, as highlighted in the box, which can be a sign of deterioration zones. From the result images, as shown in Fig. 10(b) and (d), we can notice that the proposed method detects the bright rebar hyperbolic signatures accurately, even in the attenuation zones where the rebar has less contrast.

In another example, the real GPR image has a noisy background, and the rebars are not aligned, as shown in Fig. 11(a). Despite these challenges, the rebar signatures are detected correctly with the proposed method, as shown in Fig. 11(b).

V. Bridge Deck Assessment: Case-Study Example

GPR has been widely used for the detection and location of bridge deck delamination. However, the interpretation of the large amount of acquired and stored GPR data requires the operations of well-trained civil engineers, involving thus high cost in terms of time and money. Also, such a detection method is neither reliable nor efficient. These problems have resulted in an increasingly growing demand for the development of semi- and fully automated bridge assessment techniques that are reliable, robust and rapid.

GPR data processing usually includes four phases: a) preprocessing; b) data processing; c) interpretation and visualization;

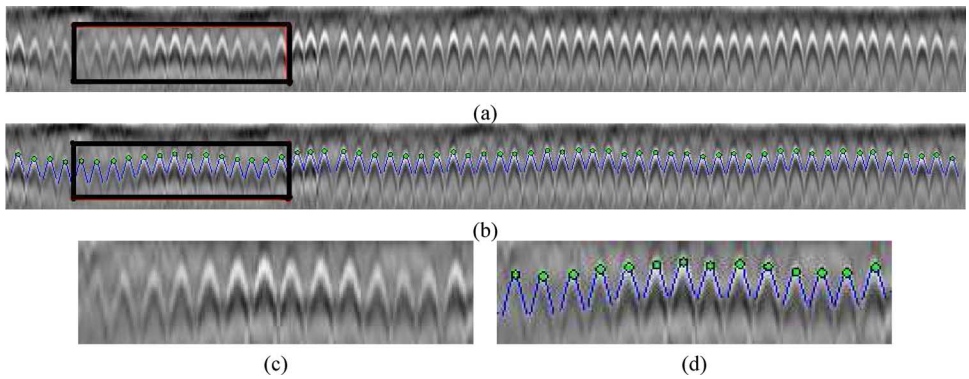

Fig. 10. Rebar detection in a GPR image. (a) Original GPR image. (b) Rebar detection result. (c) Highlighted and enlarged region in the original GPR image. (d) Highlighted and enlarged region in detection result.

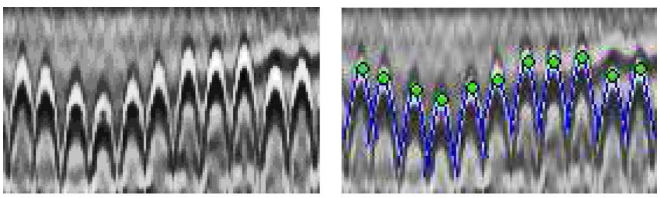

Fig. 11. Rebar detection in a GPR image. (a) Original GPR image. (b) Rebar detection result.

and d) reporting. Despite the facts that computer processors are becoming more efficient and GPR software packages are becoming more user-friendly, such as RADAN from GSSI Inc., the processing and interpretation of the GPR data from bridges is still the most time-consuming phase and an interpreter's skills play a key role in the success of a GPR project. Many of the previously mentioned GPR manufacturers are also producing software packages or modules for infrastructure surveys. Most of them, however, are designed for roads instead of bridges. Even for the bridge specific packages, such as RADAN, the current procedures leading to the final assessment report suffer from such drawbacks as excessive reliance on experienced operators' intervention and scan-by-scan processing. Also, the Bridge Assessment Module from GSSI cannot generate the final contour plot of the bridge condition. It has to rely on a third-party software package "Surfer" and a considerable amount of manual process by civil engineers, such as depth correction. Rebar amplitude signal decreases as a function of depth in the concrete since the GPR signal attenuates simply due to beam-spread and scattering. Hence, a process named "depth correction" is usually applied.

Significant improvements to the automation of a bridge condition evaluation process are expected to come from the effective use of image processing and visualization techniques. This work represents significant effort to this end. It presents an automatic detection approach of bridge deck delamination. A bridge deck in Warren County of western New Jersey is chosen as a test case to demonstrate the proposed approach.

In our study, the surveyed bridge is located at the township of Bloomsbury in Warren County of western New Jersey. Its location is shown in the map in Fig. 12. It was built and named Mu-

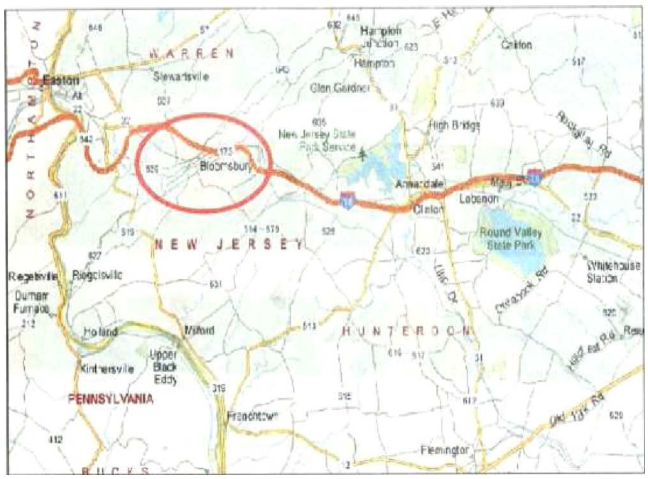

Fig. 12. Location of the bridge.

nicipal Drive Bridge over Pohatcong Creek in 1970. The bridge has a bare concrete deck, which is about 35 m (120 ft) long.

We develop a bridge assessment platform that is used to combine the 2D input GPR files into a single 3D one. Each 2D file is a cross-section GPR image slice of the bridge deck, indicative of one scan in the longitudinal direction of the bridge. We align these 2D files together to form a single 3D file, representing the internal structure of the bridge deck, which is used to generate the deterioration map. There are three major processing steps involved in creating a deterioration map from a 3D file, including rebar detection, as discussed in the previous section, depth correction and contour plot generation. Among these three components, rebar detection is the most important.

The color coded planview contour plot (deterioration map) is generated using the normalized and corrected amplitude of the reflection at the rebar level. Color levels assigned to the amplitude represent the level of attenuation and, qualitatively, the severity of deterioration. Usually, the hot colors (red, orange, and yellow) represent the severest levels of deterioration and the cool colors (blue and green) represent the low level of deterioration or a deck in a good condition. In our test case in Warren County, the contour plot of amplitude attenuation at the rebar layer is shown in Fig. 13.

For the sake of validation, experienced civil engineers also generated the corresponding deterioration map with the tradi-

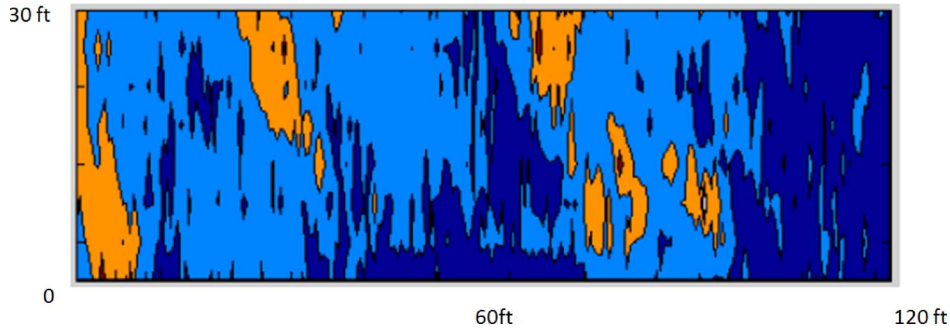

Fig. 13. Contour plot of deterioration map.

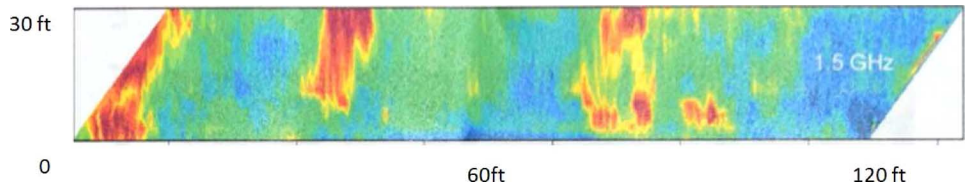

Fig. 14. Contour plot using traditional method.

tional manual method, as shown in Fig. 14. It is then compared with our results. Note that "alert" zones with hot colors in the deterioration map is of great importance for evaluating the bridge deck condition. The experts compared the maps generated with automatic and traditional methods, especially the positions and areas of the "alert" zones in two maps and validated our automatic detection approach based on the comparison results.

VI. Conclusion

Accurate bridge deck assessment is of significant importance considering that numerous bridges have been in use for a long time and thus are regularly to be examined. This paper proposes a novel method using PDEs to detect the rebar mat of bridge deck in GPR images. Our experiments have demonstrated the ability of this method to accurately detect rebars in GPR images, even for diminishing contrast and low SNR. The results presented in the paper indicate that the proposed method has much promise in automatic delamination detection of bridge decks. In future work, we are interested in testing our method with a large number of real GPR image datasets. Additional future topics can include benchmark studies with other methods such as subspace selection.

References

[1] N. Gucunski, G. Slabaugh, Z. Wang, T. Fang, and A. Maher, "Visualization and interpretation of impact echo data from bridge deck testing," in *Transportation Res. Record*, Washington, D.C., 2008, pp. 111–121.

[2] F. A. Romero, G. E. Roberts, and R. L. Roberts, "Evaluation of bridge deck survey results used for delineation and removal/maintenance quantity boundaries on asphalt-overlaid reinforced concrete deck," in *Proc. Annu. Conf. Structural Mater. Technol.*, Atlantic City, NJ, Feb. 2004, pp. 23–30.

[3] D. Huston, P. Fuhr, K. Maser, and W. Weedon, "Nondestructive testing of reinforced concrete bridges using radar imaging techniques," *Final Research Report NETC 94–2 for New England Transportation Consortium*, vol. 2, no. 1, pp. 23–31, Feb. 2000.

[4] S. Delbo, P. Gamba, and D. Roccato, "A fuzzy shell clustering approach to recognize hyperbolic signatures in subsurface radar images," *IEEE Trans. Geosci. Remote Sensing*, vol. 38, no. 3, pp. 1447–1451, May 2000.

[5] P. Gamba and S. Lossani, "Neural detection of pipe signatures in ground penetrating radar images," *IEEE Trans. Geosci. Remote Sensing*, vol. 38, no. 2, pp. 790–797, Mar. 2000.

[6] P. D. Gader, J. M. Keller, and B. N. Nelson, "Recognition technology for the detection of buried landmines," *IEEE Trans. Fuzzy Systems*, vol. 9, no. 1, pp. 31–43, Feb. 2001.

[7] P. D. Gader, B. N. Nelson, H. Frigui, G. Vaillette, and J. M. Keller, "Fuzzy logic detection of landmines with ground penetrating radar," *Signal Process.*, vol. 80, no. 6, pp. 1069–1084, 2000.

[8] W. Al-Nuaimy, Y. Huang, M. Nakhkash, M. T. C. Fang, V. T. Nguyen, and A. Eriksen, "Automatic detection of buried utilities and solid objects with GPR using neural networks and pattern recognition," *J. Appl. Geophys.*, vol. 43, no. 2-4, pp. 157–165, 2000.

[9] V. Krause, I. Abdel-Qader, O. Abudayyeh, and S. Yehia, "An image segmentation algorithm for the detection of rebar in bridge decks from GPR scans," in *Proc. IEEE Int. Conf. Electro Information Technol.*, Chicago, IL, May 2007, pp. 114–119.

[10] R. Morey, "Ground penetrating radar for evaluating subsurface conditions for transportation facilities," *Synthesis of Highway Practice 255, National Cooperative Highway Research Program, Transportation Research Board*, 1998.

[11] R. M. Morey and A. Kovacs, "Detection of moisture in construction materials," CRREL (Cold Region Research and Engineering Laboratory), Hannover, NH, Tech. Rep. 77-25, 1977.

[12] T. Cantor and C. Kneeter, "Radar and acoustic emission applied to study of bridge deck, suspension cables and masonry tunnel," *Transportation Res. Record 676*, vol. 67, no. 6, pp. 31–42, 1978.

[13] T. Scullion, C. L. Lau, and Y. Chen, "Pavement evaluations using ground penetrating radar," in *Proc. Int. Conf. Ground Penetrating Radar*, Kitchener, ON, Canada, Jun. 1994, pp. 449–463.

[14] K. R. Maser and T. Scullion, "Automated detection of pavement layer thicknesses and subsurface moisture using ground penetrating radar," *Transportation Res. Record 676*, pp. 165–172, 1978.

[15] X. Zeng, G. A. McMechan, J. Cai, and H. W. Chen, "Comparison of Ray and Fourier methods for modeling monostatic ground-penetrating radar profiles," *Geophysics*, vol. 60, no. 6, pp. 1727–1734, 1995.

[16] J. M. Bourgeois and G. S. Smit, "A fully three-dimensional simulation of a ground-penetrating radar," *IEEE Trans. Geosci. Remote Sensing*, vol. 34, no. 1, pp. 36–44, Jan. 1996.

[17] P. Kolisoja, N. Vuorimies, and T. Saarenketo, "Assessment of the effect of seasonal variations on the unbound materials of low volume roads," in *Proc. Int. Symp. Pavements Unbound*, Nottingham, U.K., Jul. 2004.

[18] F. A. Romero and R. L. Roberts, "Data collection, processing and analysis challenges-GPR bridge deck deterioration assessment of two unique bridge deck systems," in *Proc. Symp. Appl. Geophys. Environmental and Engineering Problems (SAGEEP)*, 2004.

[19] W. Al-Nuaimy, Y. Huang, and S. Shihab, "Automatic target detection in GPR data," in *Proc. Int. Conf. Ground Penetrating Radar*, Santa Barbara, CA, 2002, pp. 139–143.

Zhe Wendy Wang (M'09) received the B.E. degree in electronics engineering from Tsinghua University, Beijing, China, the M.E. degree from the Chinese Academy of Science, Beijing, in electronics engineering, and the Ph.D. degree from the Department of Electrical and Computer Engineering, New Jersey Institute of Technology, Newark.

She is now working for IRIS ID Inc. (formerly LG IRIS Dept.), Cranbury, NJ. Prior to that, she has worked for Siemens Corporate Research, Princeton, and Thomson Corporate Research, Princeton. Her research interests include image/video processing and analysis.

Mengchu Zhou (S'88–M'90–SM'93–F'03) received the B.S. degree in electrical engineering from Nanjing University of Science and Technology, Nanjing, China, in 1983, the M.S. degree in automatic control from Beijing Institute of Technology, Beijing, China, in 1986, and the Ph.D. degree in computer and systems engineering from the Rensselaer Polytechnic Institute, Troy, NY, in 1990.

He joined the New Jersey Institute of Technology (NJIT), Newark, in 1990, and is currently a Professor of Electrical and Computer Engineering and the Director of Discrete-Event Systems Laboratory. He is presently a Professor at The Key Laboratory of Embedded System and Service Computing, Tongji University, Shanghai, China (on leave from NJIT). He was invited to lecture in Australia, Canada, China, France, Germany, Hong Kong, Italy, Japan, Korea, Mexico, Singapore, Taiwan and the U.S. and served as a plenary speaker for several conferences. He has led or participated in 40 research and education projects with total budget over $10 M, funded by National Science Foundation, Department of Defense, Engineering Foundation, New Jersey Science and Technology Commission, and industry. He has over 360 publications including 10 books, 160+ journal papers (majority in IEEE TRANSACTIONS), and 17 book chapters. He recently coauthored *Modeling and Control of Discrete Event Dynamic Systems*, Springer, London, 2007 (with B. Hruz), *Deadlock Resolution in Automated Manufacturing Systems: A Novel Petri Net Approach*, Springer, New York, 2009 (with Z. Li), and *System Modeling and Control with Resource-Oriented Petri Nets*, CRC Press, New York, 2010 (with N. Wu). His research interests are in intelligent automation, lifecycle engineering and sustainability evaluation, Petri nets, wireless ad hoc and sensor networks, semiconductor manufacturing, and energy systems.

Prof. Zhou was the recipient of NSF's Research Initiation Award, CIM University-LEAD Award by the Society of Manufacturing Engineers, the Perlis Research Award by NJIT, the Humboldt Research Award for U.S. Senior Scientists, the Leadership Award and Academic Achievement Award by the Chinese Association for Science and Technology-USA, the Asian American Achievement Award by the Asian American Heritage Council of New Jersey, and the Distinguished Lecturership of the IEEE SMC Society. He was the Founding Chair of the Discrete-Event Systems Technical Committee and Founding Co-Chair of the Enterprise Information Systems Technical Committee of the IEEE SMC Society, and Chair (founding) of the Semiconductor Manufacturing Automation Technical Committee of the IEEE Robotics and Automation Society. He is a Life Member of the Chinese Association for Science and Technology-USA and served as its President in 1999. He served as an Associate Editor of the IEEE TRANSACTIONS ON ROBOTICS AND AUTOMATION from 1997 to 2000, and the IEEE TRANSACTIONS ON AUTOMATION SCIENCE AND ENGINEERING from 2004–2007, and is currently an Editor of the IEEE TRANSACTIONS ON AUTOMATION SCIENCE AND ENGINEERING, and an Associate Editor of the IEEE TRANSACTIONS ON SYSTEMS, MAN AND CYBERNETICS: PART A, and the IEEE TRANSACTIONS ON INDUSTRIAL INFORMATICS. He served as a Guest Editor for many journals including the IEEE TRANSACTIONS ON INDUSTRIAL ELECTRONICS and the IEEE TRANSACTIONS ON SEMICONDUCTOR MANUFACTURING. He was General Chair of the IEEE Conference on Automation Science and Engineering, Washington DC, August 23–26, 2008, General Co-Chair of the 2003 IEEE International Conference on System, Man and Cybernetics (SMC), Washington DC, October 5–8, 2003, Founding General Co-Chair of the 2004 IEEE International Conference on Networking, Sensing and Control, Taipei, March 21–23, 2004, and General Chair of the 2006 IEEE International Conference on Networking, Sensing and Control, Ft. Lauderdale, FL, April 23–25, 2006. He was Program Chair of the 2010 IEEE International Conference on Mechatronics and Automation, August 4–7, 2010, Xian, China, the 1998 and 2001 IEEE International Conference on SMC and the 1997 IEEE International Conference on Emerging Technologies and Factory Automation. He organized and chaired over 80 technical sessions and served on program committees for many conferences.

Gregory G. Slabaugh (M'02–SM'08) received the Ph.D. degree in electrical engineering from the Georgia Institute of Technology, Atlanta.

He is the Head of Research and Development at Medicsight PLC, an industry leader in computer-aided detection software in medical imaging. He held positions at Hewlett-Packard Laboratories and Siemens Corporate Research. He has over 60 publications and over 30 patents pending in the fields of computer vision and medical image processing; in particular, his research interests include computer-aided detection, image segmentation, registration, geometric modeling, multiview stereo, adaptive filtering, and partial differential equations.

Dr. Slabaugh is an Associate Editor of the IEEE *Signal Processing Magazine*. He co-organized the International Workshop on Computer Vision for Intravascular and Intracardiac Imaging held in conjunction with MICCAI 2006. He served as a Guest Associate Editor for a Special Issue of the IEEE TRANSACTIONS ON INFORMATION TECHNOLOGY IN BIOMEDICINE on the same topic.

Jiefu Zhai (M'09) received the B.E. degree in electrical engineering from Xi'an Jiaotong University, Xi'an, China, in 2001, and the M.S. degree in computer engineering from the Institute of Computing Technology, Chinese Academy of Sciences, Beijing.

He was with Thomson Corporate Research, Princeton, NJ, from 2004 to 2010, and is now with Apple Inc., Cupertino CA. His research interests are in the areas of video processing and video compression.

Tong Fang received the M.Sc degree in management science from the University of Science and Technology, Beijing, China, in 1992, the M.Sc. degrees in industrial engineering in 1997 and in electrical and computer engineering in 1999, respectively, and the Ph.D. degree in 2000 from Rutgers University, Piscataway, NJ.

He is currently a Research Scientist and Manager of Adaptive Techniques R&D Program at Siemens Corporate Research, Princeton, NJ. His current research interests include medical image processing, geometric modeling, and visualization.